# High-Resolution Portable Dual-Point Liquid Level Measurement System Using POF

Muhammad Saleh Urf Kumail Haider, Chen Chen, Senior Member, IEEE, Abdul Ghaffar, Laraib Unsa Noor, Sadam Hussain, and Min Liu

Abstract—This paper presents a portable dual-point optical fiber sensor system for continuous liquid level measurement using polymer optical fibers (POFs). The system contains sensor design and integration with smartphone. The sensor design employs a twisted coupling technique, where two bare optical fibers are twisted together, allowing power to transfer from the illumination fiber to the coupled fiber. The 3D-printed casing mounts into smartphone where the sensor system is attached to casing. The light is launched from the smartphone's flashlight and next end of fiber is to the camera. The flashlight serves as the light source, and the camera records intensity variations caused by changes in the liquid level. Experimental results demonstrate a linear response in optical power intensity as liquid levels increase, allowing for precise measurement of levels up to 120 mm simultaneously. Sensor-1 achieved a sensitivity of 0.050%/mm and sensor-2 exhibited a sensitivity of 0.033%/mm, with a resolution of 0.05 mm. Both sensors showed stable and consistent performance during ascent and descent phases of liquid level measurement. This cost-effective, portable sensor system offers high accuracy and reliability, making it suitable for industrial applications such as chemical processing and environmental monitoring.

Index Terms—Portable sensor, smartphone, dual-sensor, liquid level measurement, polymer optical fiber (POF), coupling.

## I. INTRODUCTION

THE portable liquid level sensor offers a precise and reliable solution for monitoring liquid levels across various sectors. It is particularly useful in applications like oil transportation, dam safety assessments, and managing underground reservoirs. The POF sensors effectively detects and quantifies liquid level variations, which is critical for ensuring safety and operational efficiency. Whereas traditional electrical and mechanical liquid level measurement devices, such as float systems [1], pressure transducers [2], hydrostatic level sensors [3], ultrasonic sensors [4], radar level sensors [5], and capacitance level sensors [6], [7], often face limitations in precision, maintenance, and complexity for being, especially in harsh environments. These systems may not provide the

This research was supported by the National Natural Science Foundation of China under Grant 61901065, and in part by the Natural Science Foundation of Chongqing under Grant cstc2021jcyj-msxmX0480.(Corresponding author: Chen Chen)

Muhammad Saleh Urf Kumail Haider, Chen Chen, Laraib Unsa Noor, and Min Liu are with the School of Microelectronics and Communication Engineering, Chongqing University, Chongqing 400044, China (e-mail: kumailsandano@gmail.com; c.chen@cqu.edu.cn; laraibunsanoor@gmail.com; liumin@cqu.edu.cn).

Abdul Ghaffar and Saddam Hussain are with the Key Laboratory of Air-Driven Equipment Technology of Zhejiang Province, College of Mechanical Engineering, Quzhou University, Quzhou 32400, Zhejiang, China (e-mail: ghaffar@qzc.edu.cn; sadamhussain@qzc.edu.cn).

level of accuracy or ease of use needed for more demanding applications. The advancements of the research for optical fiber sensors (OFSs) present an attractive alternative to conventional measurement techniques due to their high responsiveness, compact size, cost-effectiveness, and the ability to work in harsh environments [8], [9]. Most importantly there multiparameter sensing capabilities in OFSs like liquid level with saltiness of sea water [10]–[12], temperature [13], [14], refractive index [15], [16], and pH detection makes them an ideal choice for a broad spectrum of industries and household applications [17], [18].

The OFS typically relies on either silica optical fibers (SOFs) or polymer optical fibers (POFs) [19]. The SOF sensors use wavelength modulation techniques like fiber Bragg gratings [20], [21], long-period gratings [22], [23], and Mach-Zehnder interferometers [24], [25], offering high accuracy but at a higher cost and with increased fragility. This makes SOFs less suitable for applications that require durability and flexibility, especially in techniques that rely on optical power attenuation or bend loss [6], [26]. In contrast, POFs are more flexible, have higher attenuation for visible light, and feature a larger core diameter, making them ideal for liquid level sensing applications [27], [28]. Several studies have proposed singlepoint sensing techniques for example, Park et al. [29] proposed a sensor with micro-holes for liquid level sensing. Similarly, the Zhang et al. [30] fabricated a liquid level sensor capable of sensing depth at discrete points using a coupling method. Liao et al. [31] proposed POF based liquid level sensor with spiral micro bending the sensor was twisted around a column, extended the capability for liquid level depth sensing although its resolution was relatively low. However, methods such as micro-drilling, grooving, and chemical etching enhance the sensor's responsiveness to the surrounding medium; nonetheless, these approaches compromise the sensor's durability and complicate the fabrication process. These physical machining methods often lead to stress concentrations and potential micro-cracks, which reduce mechanical durability and longterm reliability, especially in harsh environments involving chemical exposure or humidity variations.

The demand for portable sensors is increasing rapidly due to their numerous advantages. The integration of POF sensors with smartphones streamlines equipment requirements, rendering it a feasible and efficient option [32]–[34]. Recent advancements in smartphone technology have facilitated its integration with diverse scientific applications owing to improved computational ability and optical imaging capabilities. In the realm of portable sensors, Ye et al. [35] developed a

portable multi-hole POF sensor for liquid level measurement. However, the drilling step added complexity to the setup, limiting its ability to provide continuous and precise liquid level measurements. While the system can detect liquid at specific points, it does not offer full continuous liquid level sensing. Another study explored a multiparameter sensor for liquid level and refractive index [36], using two different techniques: a notched POF with a U-shaped sensor structure. This sensor achieved maximum sensitivity for liquid level sensing but had a lower resolution of 30 mm over a 90 mm sensing range, which is less precise compared to existing solutions, but the system was limited to single-point detection.

Despite these advancements in existing liquid level sensors, while effective in their respective applications, often fall short in terms of portability and dual-sensor capabilities. Many existing sensors require complex setups, external power sources, and dedicated control units for fixed installations. These factors make them less suitable for mobile or remote applications where portability and ease of use are crucial. Furthermore, most portable liquid level sensors focus on single-point measurements, which may not provide the real-time data needed for more complex environments for multipoint liquid level detection. The multipoint sensor liquid level has remained largely unexplored.

In this work, we for the first time propose a portable, high-resolution dual-sensor liquid level measurement system using POFs and a smartphone. The system integrates two bared POFs: one connected to the smartphone's flashlight as a light source and the other to its camera to detect light intensity variations. The sensor design operates on the simple principle of twisting and coupling phenomena, where changes in the refractive index due to the liquid level variations affect the light transmission through the fibers. This straightforward design not only simplifies the setup but also ensures real-time data collection and analysis. The dual-sensor setup captures variations at two points, providing more accurate and reliable measurements for a comprehensive understanding of liquid levels. The portability and user-friendly nature of this system makes it ideal for a wide range of applications, from industrial monitoring to environmental sensing. It enhances the overall efficiency and reliability of liquid level measurements, offering a practical and advanced solution for modern sensing needs. A detailed description of the sensor design and theory implementation is presented in Section 2. Section 3 highlights the results obtained and the discussions, while Section 4 mentions the overall conclusions and future applications.

## II. METHODOLOGY

# A. Sensor Fabrication

The proposed sensor design for measuring liquid level employs a technique utilizing twisting coupled structures with POFs. Specifically, the study uses step-index SK-40 fibers with a core diameter of 980  $\mu$ m and a cladding thickness of 10  $\mu$ m. The refractive index contrast between the core (1.49) and the cladding (1.41) ensures efficient light guidance via total internal reflection. The flexibility of the SK-40 fibers facilitates the implementation of the twisting and coupling processes necessary for the sensor's operation.

The sensing system is configured with a single illumination fiber (IF) and two coupled fibers (CFs) designated as CF-1 and CF-2 for dual-point liquid level sensing. This configuration enables independent liquid level measurement at two distinct points using a single light source. Both CF-1 and CF-2 are integrated onto the primary IF. The initial point of the IF is connected to the light input source, where the IF is first twisted with CF-1 to create the sensor-1 probe, followed by twisting the same IF with CF-2 to create the sensor-2 probe. To achieve independent liquid level measurement, the terminal ends of CF-1 and CF-2 are interfaced with smartphone cameras. To ensure uniform twisting across sensors, we chose the commercially available twisting machine, as shown in Fig. 1(b). This machine provides precise control over the twisting process, allowing for consistent application of tension and speed. These fabricated sensors have the same twist rate for both sensors, with 1 twist per centimeter, ensuring uniformity in the measurement system. The dual-sensor liquid level measurement system operates on the principle of detecting liquid level variations based on optical power intensity variations.

## B. Theory

In this study, we present a comprehensive theoretical framework for a dual-sensor liquid level measurement system. The model employs a single IF coupled with two multimode optical fibers, and it is grounded in classical coupled-mode theory. The schematic representation of the sensor configurations is depicted in Fig. 1(a). The efficiency of power coupling between the fibers is influenced by parameters such as the separation distance d, the material properties of the fibers, and the surrounding medium, including the liquid. The power coupling varies as the liquid level rises due to the absorptive properties of the liquid. As the liquid level increases, the power transferred from the IF to the CF decreases, correlating directly with the length of the submerged fiber segment. The power in the IF  $P_0(x)$  and the power in the CF  $P_1(x)$  follow a set of first-order differential equations. When the light enters the system through an input port  $P_{in}$ , the IF propagates the light. The CF propagates the coupled power denoted as  $P_{out}$ . The output power at the IF is denoted as  $P_0$  while the output power at the CF-1 is denoted as  $P_1$  for liquid level sensor. The power transfer dynamics between the two fibers can be described by a set of coupled differential equations [37], [38]:

$$\begin{cases} \frac{d}{dx}P_0(x) = -(\alpha_0 + \beta_0(L))P_0(x) + \beta_0(L)P_1(x) \\ \frac{d}{dx}P_1(x) = \beta_0(L)P_0(x) - (\alpha_1 + \beta_0(L))P_1(x) \end{cases}$$
(1)

where  $P_0(x)$  is the power in IF;  $P_1(x)$  is the power in CF;  $\alpha_0$  and  $\alpha_1$  represent the attenuation coefficients of the fibers, while  $\beta_0(L)$  is the coupling coefficient, which depends on the liquid level L and x is the distance. Here, the attenuation is assumed to be equal because both IF and CFs are taken as the same type of fiber and while Equation (1) expresses a straightforward intuitive concept. To grasp its essence, Fig. 1(a), offers an interpretative visualization in sensor-1 through a power balance perspective, akin to a finite-difference equation paralleling (1) applied to a minuscule segment of length  $\Delta x$ .

$$\beta_0(L) = \beta_{\text{dry}} + \Delta \beta_{\text{wet}} \cdot \frac{L}{L_{\text{max}}}$$
 (2)

where  $L_{\rm max}$  represents the sensor's maximum operational range, while  $\beta_{\rm dry}$  represents the coupling coefficient in the dry region (no liquid), and  $\Delta\beta_{\rm wet}$  accounts for the change in coupling liquid level ascent or descent.

The boundary conditions for this system are set such that at the input of the illuminating fiber,  $P_0(0)=P_{\rm in}$  and at the start of the secondary fiber,  $P_1(0)=0$ . Solving these differential equations provides the general solutions for power in the two fibers: In this model, the initial power  $P_0$  is introduced at the start of the IF (x=0), and the resulting output power  $P_{\rm out}$  is measured at the end of the CF  $(x=L_{\rm max})$ . The solutions to the differential equations (1) under the boundary conditions for this system are set such that at the input of the illuminating fiber,  $P_0(0)=P_{\rm in}$  and at the start of the secondary fiber,  $P_1(0)=0$ , yield the power distributions along the fibers:

$$\begin{cases} P_0(x) = P_{\text{in}} \left( \frac{1 + e^{-2\beta_0(L)x}}{2} \right) e^{-\alpha_0 x} \\ P_1(x) = P_{\text{in}} \left( \frac{1 - e^{-2\beta_0(L)x}}{2} \right) e^{-\alpha_1 x} \end{cases}$$
(3)

At the endpoint  $L_{\rm max}-L$ , which represents the region where the liquid level affects coupling, the power in the secondary fiber becomes:

$$P_1(L_{\text{max}} - L) = P_{\text{in}}\left(\frac{1 - e^{-2\beta_0(L)(L_{\text{max}} - L)}}{2}\right)e^{-\alpha_1(L_{\text{max}} - L)}$$
(4)

To determine the output power at the end of the secondary fiber, considering the fiber attenuation, the final equation for liquid level sensing is:

$$P_{\text{out}}(L) = P_1(L_{\text{max}} - L)e^{-\alpha_1 L} \tag{5}$$

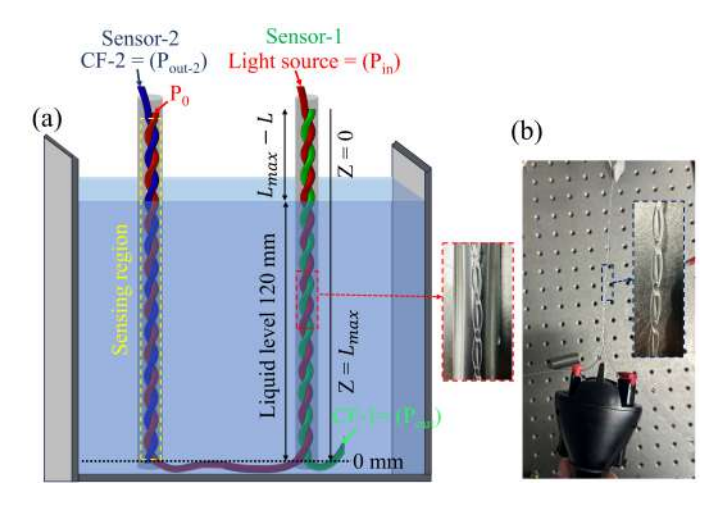
By substituting the values of  $P_1(L_{\text{max}} - L)$ , we arrive at the final output power equation:

$$P_{\text{out}}(L) = P_{\text{in}}\left(\frac{1 - e^{-2\beta_0(L)(L_{\text{max}} - L)}}{2}\right)e^{-\alpha_0 L_{\text{max}}}$$
 (6)

This equation shows how the output power decreases as the liquid level L increases. In the region where the liquid is highly absorptive, i.e.,  $\Delta x = \{x: L_{\max} - L < x < L_{\max}\}$ , the coupling coefficient  $\beta_0(L)$  becomes negligible, resulting in a simplified expression for  $P_{\text{out}}$  that reflects the direct impact of liquid absorption on the transmitted light. This condition rationalizes the presence of the term  $e^{-\alpha_0 L}$  in equation (6).

## C. Parameters for Model Configuration

In our sensor design, we consider the attenuation coefficient  $\alpha$ , which includes both absorption and scattering losses, to play a critical role in determining the overall performance of the optical fibers. The SK-40 fiber attenuation losses can reach as high as  $0.15\,\mathrm{dB\,m^{-1}}$ , which corresponds to a higher  $\alpha$  value to accurately represent these effects in our model [39]. This



3

Fig. 1. (a) Schematic diagram of dual-sensor based liquid level measurement and (b) twisting machine for uniform fiber twisting.

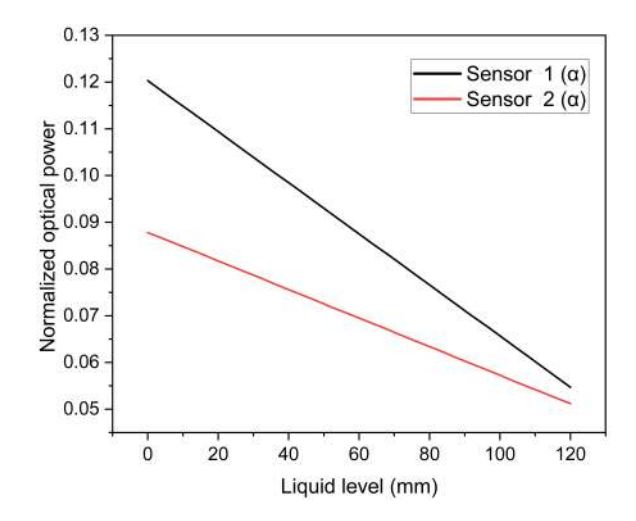


Fig. 2. Theoretical results of liquid level vs normalized optical power due to coupling effect.

ensures that the sensor operates effectively, even at greater depths and longer fibers. The coupling coefficient  $\beta_0(L)$  on the other hand, depends on both the geometrical and optical properties of the fibers. Specifically, the separation distance d between the IF and the CF plays a significant role. When  $d \gg \lambda$ , where  $\lambda$  is the wavelength of light, the IF emits power over a wide solid angle. As a result, only a small portion of the emitted light is coupled into the CF, which leads to a weak coupling regime, characterized by  $\beta_0(L) \ll 1 \, \mathrm{m}^{-1}$ . This weak coupling significantly influences the performance of the sensor in terms of sensitivity and linearity.

The primary equation for the power exchange between the fibers remains the same, where  $\beta_0(L)$  is the coupling coefficient, which varies with the liquid level L, and  $\alpha_0$  is the attenuation coefficient for the illuminating fiber. Given that our sensor is designed to detect liquid levels up to  $120\,\mathrm{mm}$ , we set the maximum measurable liquid level  $L_{\mathrm{max}}=120\,\mathrm{mm}$ . For modeling purposes, we explore the normalized output power,  $P_{\mathrm{out}}/P_{\mathrm{in}}$ , as a function of the liquid level using the following expression derived from our theoretical model,

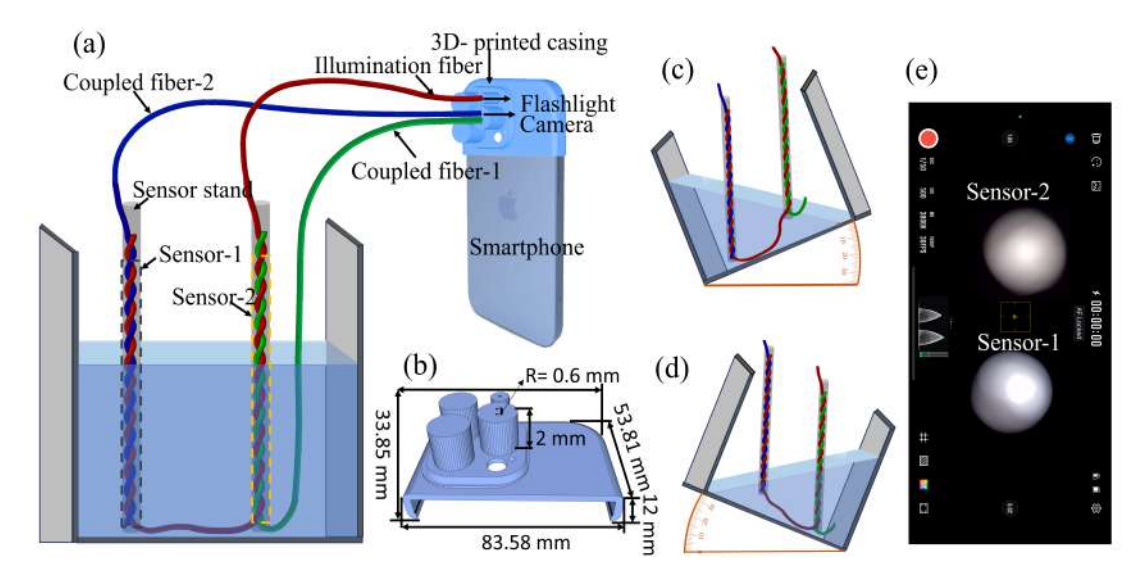


Fig. 3. The complete experimental setup. (a) shows the portable dual sensor-based liquid level measurement system. (b) the 3D-printed smartphone casing. (c) -35° left tiled liquid tank to create the uneven surface measurement system. (d) similarly, 35° right tiled. (e) is the smartphone screenshot while recording the both sensors data.

# shown in Fig. 2.

In this analysis, we assume a weak coupling scenario where  $\beta_0(L)=0.01\,\mathrm{m}^{-1}$  and the attenuation coefficient  $\alpha_0$  varies between  $0.5\,\mathrm{m}^{-1}$  and  $3\,\mathrm{m}^{-1}$ . For different values of  $\alpha_0$ , the output power is graphed against the liquid level L. The resulting graph reveals a nearly linear relationship between the liquid level and output power, as shown in Fig. 2. The linearity arises because, when  $\beta_0(L)\ll 1$ , the influence of  $\alpha_0$  on the slope of the linear relationship becomes negligible. This ensures that the sensor maintains consistent sensitivity, allowing for easy calibration and robust performance across varying environmental conditions.

#### D. Experimental Setup

The experimental setup was designed to utilize the integrated functionalities of a smartphone, particularly focusing on its camera and LED flashlight to monitor changes in light intensity for sensing variations in liquid levels. As depicted in Fig. 3(a), the smartphone served dual roles: generating light through its flashlight feature and concurrently capturing this light via the camera, while also processing the resultant data. The POF liquid level sensor's starting and ending regions were secured using nylon zip ties to ensure stability. The IF and coupled CF were connected into a 3D-printed smartphone casing, as shown in Fig. 3(b). Where IF interfacing with the smartphone's flashlight and both CFs with the camera. In the setup, the twisting coupling extended over 120 mm, and the total length of the fiber is 1.5 m for the length of all three pieces. To measure the liquid level, both liquid level sensors were placed parallel to each other and attached to metal rods within the liquid tank. The sensors were aligned with the depth scale of a vernier caliper, facilitating accurate depth readings. Calibration began by carefully submerging the sensors, ensuring precise measurements. This setup allowed for reliable and accurate monitoring of the liquid level.

We used the StaCam app which facilitates the video recording, enabling users to customize video recording settings such as light sensitivity (ISO) and exposure time. Adjusting ISO sensitivity is critical; however, excessively high settings can introduce unwanted noise, potentially compromising measurement integrity. Shutter speed calibration is equally important, as it controls light exposure and prevents intensity readings from becoming too low under noiseless ISO configurations. It is important to note that these settings are not static but require customization based on varying environmental conditions.

After recording, the video is processed frame-by-frame using MATLAB to analyze both sensors simultaneously. The video recorded with a 9:16 aspect ratio is first cropped into two equal halves: the right half corresponding to sensor-1 and the left half corresponding to sensor-2. As shown in Fig. 3(e), the brightest spot on the right side represents sensor-1, while the left side corresponds to sensor-2. The video is split from the middle, and each half is converted to grayscale using the 'rgb2gray' function. This conversion translates color information into gray values, representing brightness levels.

For each sensor, the total light intensity is calculated separately by summing the gray values of all pixels in the respective halves of the frame. The right half, representing sensor-1, computes total intensity from the midpoint of the frame to the right edge, while the left half, representing sensor-2, computes from the left edge to the midpoint. Given a video resolution of  $1920 \times 1080$ , the midpoint occurs at 960 pixels horizontally. The total intensity for each sensor is expressed as follows:

$$I_{\text{total}_1} = \sum_{i=1}^{a} \sum_{j=\frac{b}{2}+1}^{b} I_{\text{gray}}(i,j), \quad I_{\text{total}_2} = \sum_{i=1}^{a} \sum_{j=1}^{\frac{b}{2}} I_{\text{gray}}(i,j)$$
(7)

where  $I_{\text{total}_1}$  and  $I_{\text{total}_2}$  represent the total intensities for sensor-1 and sensor-2, respectively, and a and b are the dimensions of the frame. Next, the absolute intensity for both

sensors is normalized by setting the zero-level baseline at the point where the sensing area is fully immersed in the liquid. The normalized intensity for each sensor is calculated using the same equation as:  $I=I_0/I_h$ , represents the absolute intensity value at the reference zero-level position and  $I_h$  denotes the corresponding value at a specific height h. The differential intensity metric introduced to quantify changes in intensity is given by:  $\Delta I=(I_h-I_0)/I_0\times 100\%$ . This unified approach simplifies the analysis and allows real-time monitoring of intensity changes in both sensors.

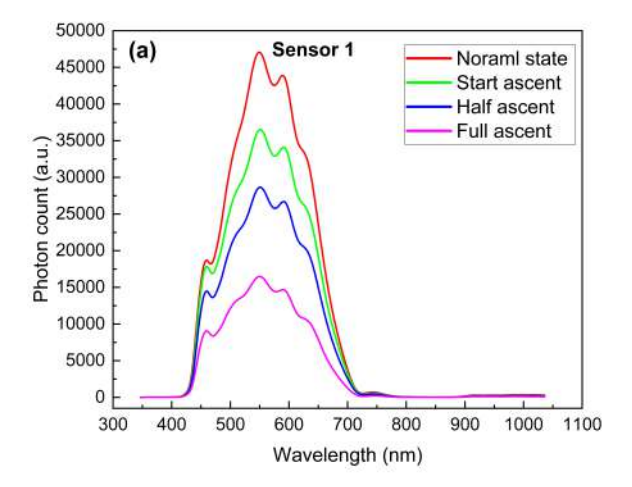
# E. Spectral Response

The experiment aimed to analyze the spectral behavior of portable dual-sensor liquid level measurement under different immersion conditions using a smartphone's flashlight as the light source and (Ocean Optics USB2000+) spectrometer for data collection. The smartphones have a maximum flashlight brightness of approximately 600 nits (candela per square meter), providing a consistent and bright light source for the experiment. The spectral range of the smartphone's flashlight typically covers wavelengths from around 450 nm to 650 nm [40], [41], encompassing the visible light spectrum predominantly within the blue to red regions. Initially, the sensors were tested in normal state in refractive index (air  $\approx$  1), establishing a baseline response, as shown in Fig. 4. We measure the spectral response at four stages: the normal state as the reference point, the ascended sensor at a depth of 1 mm to half, and finally the fully ascended state. Fig. 4(a) shows the response of sensor-1, and Fig. 4(b) shows the response of sensor-2 at four different stages. Upon partial submersion, the spectral signatures exhibited significant attenuation, indicating an interaction between the sensors and the liquid-air interface. When fully submerged, the sensors demonstrated a marked alteration in their spectral responses, reflecting a strong optical interaction with the liquid. These findings suggest that the sensors can effectively differentiate between air and liquid phases, making them suitable for liquid level detection.

## III. RESULTS AND DISCUSSION

The dual-point based portable liquid level measurement system is employed to measure and monitor variations in liquid level at uneven surfaces or varying locations. The measurement response correlates the coupled intensity variation with the liquid level in millimeters (mm). All results from the dual-point sensor were obtained at a room temperature of 25 °C. The experiment illustrates the response of a dual-point liquid level sensor for continuously ascending and descending liquid levels.

Fig. 5(a) depicts the simultaneous ascending of both sensors' responses with respect to time. We consider the response of Sensor-1 as the reference point for the ascending phase on static or even surfaces. Fig. 5(b) shows the simultaneous response of both sensors during the descending phase, demonstrating that the coupled power intensity increases as the liquid level descends continuously. It is worth noting that the sensors exhibit a slower response time when the liquid level decreases compared to when it increases. This difference



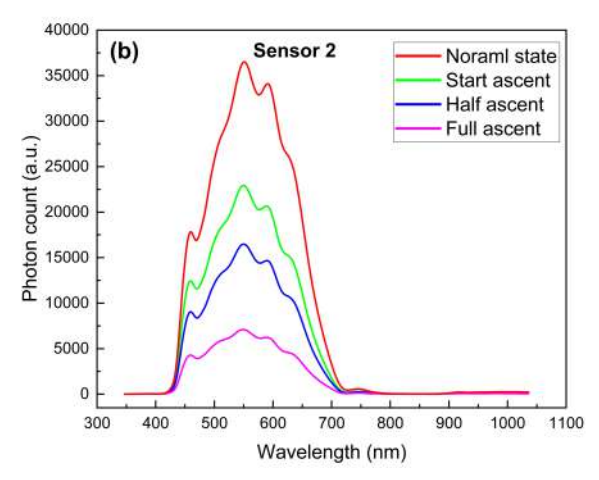
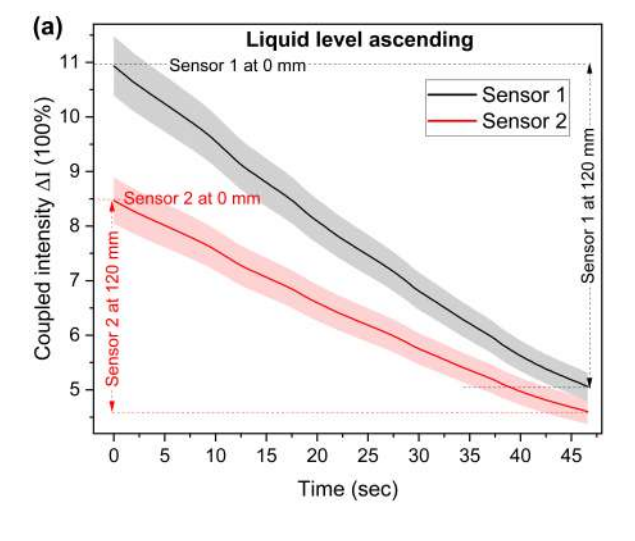


Fig. 4. The spectral response of portable dual-sensor liquid level measurement with flashlight source at four different stages. (a) sensor-1 response in normal state, start, half and fully ascended in liquid and (b) shows the spectral response of sensor-2.

is primarily due to the sensor's wettability. When the liquid level drops, the sensors remain wet, causing the refractive index to change more gradually during the decrease in liquid level. Throughout the test cycles, the sensors demonstrated reliable and repeatable responses, indicating their suitability for detecting precise changes in liquid levels, even under dynamic conditions. The constant flow rate ensured that the observed variations were attributed solely to changes in the liquid level rather than flow dynamics, thus validating the reliability of the sensors in real-world applications where liquid levels may fluctuate frequently.

Additionally, it is worth noting that the initial power coupling of both sensors may vary that depends on the twisting conditions. If there is perfectly aligned, then the initial power coupling will be remains same. Furthermore, sensor-1 has a higher input light intensity than sensor-2 because the light firstly propagates through sensor-1 and loss some power. A reduced power reached to the Sensor-2 from total power. However, both sensors show the same response to changes in the liquid level.

Fig. 6 demonstrates that the sensors register changes as a reduction in optical power intensity as the liquid level rises. This reduction in optical power intensity is attributed to the



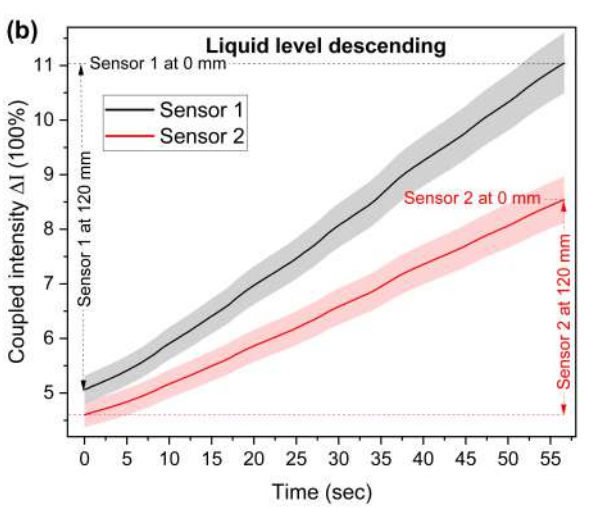
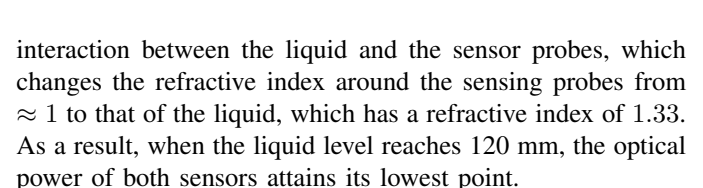
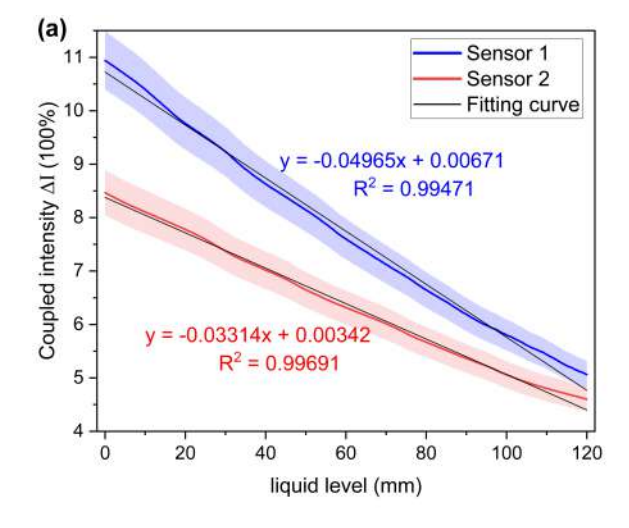


Fig. 5. Dual-sensor liquid level measurement response over time with mean absolute error of  $\pm 5\%$ , (a) liquid level ascending, (b) liquid level descending.



The responses of both sensors to liquid level measurements are depicted in Fig. 6(a). Both sensors display a linear decrease in optical power intensity as the liquid level ascends, with the capability to detect levels up to 120 mm, which matches the length of the fabricated sensor probes. For Sensor-1, the R-squared value is 0.99471, with a sensitivity of 0.049%/mm and a resolution of 0.05mm, whereas for Sensor-2, the R-squared value is 0.99691, with a sensitivity of 0.033%/mm and a resolution of 0.05mm. Similarly when the liquid level decreases, both sensors show a linear increase in optical power intensity, maintaining their linearity and reliability as shown in the Fig. 6(b).

Fig. 7(a)(b) showcases the consistent response of the dualsensor liquid level measurement during continuous ascending and descending in liquid levels. Throughout these repeated sensing cycles, both sensors demonstrate stable and compa-



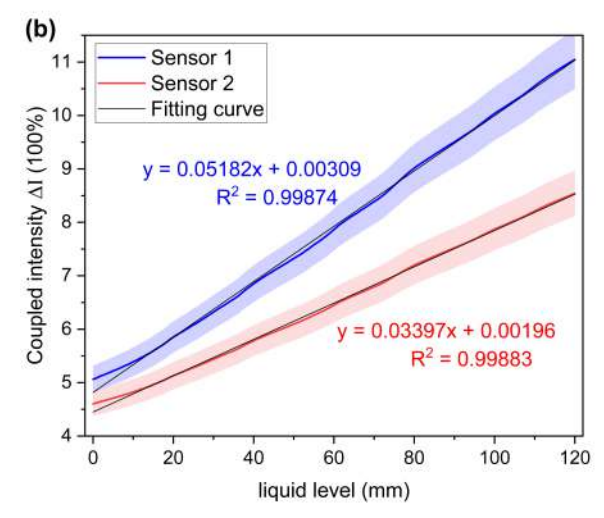
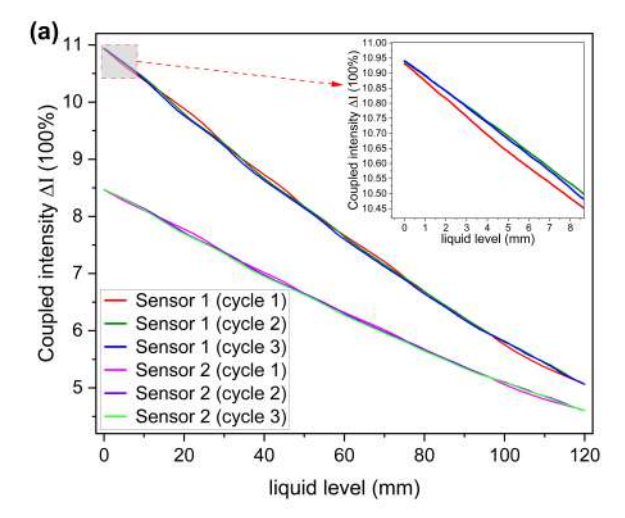


Fig. 6. Dual-sensor response with mean absolute error of  $\pm 5\%$ , (a) sensors ascending response with respect to level in mm and (b) sensors response while descending.

rable reactions to changes in the liquid level, regardless of whether the level is rising or falling. The repetitive sensor response curve effectively highlights the sensors' capabilities across multiple trials. The experimental findings are summarized in Table I, indicating sensor-1 sensitivity with an average value of  $0.050 \pm 0.005$  %/mm during the ascent phase and  $0.051 \pm 0.009\%$ /mm during the descent phase while the sensor-2 with an average value of  $0.032 \pm 0.004$  %/mm during the ascent phase and  $0.033 \pm 0.004$  %/mm during the descent phase. These graphs show that across multiple tests, both sensors are responsive to changes in the liquid level, whether it is increasing or decreasing liquid levels. This consistency suggests that the dual-sensor liquid level measurement maintains similar characteristics and sensitivities, ensuring reliable performance whether the liquid level is rising or falling. Overall, the repetitive sensor response curve emphasizes the ability of the proposed portable high-resolution dual-sensor liquid level measurement system to provide consistent and highly repeatable responses to changes in the liquid level.

Fig. 8(a)(b), illustrates the response of the dual-point liquid level sensor under uneven ground conditions. The experimen-



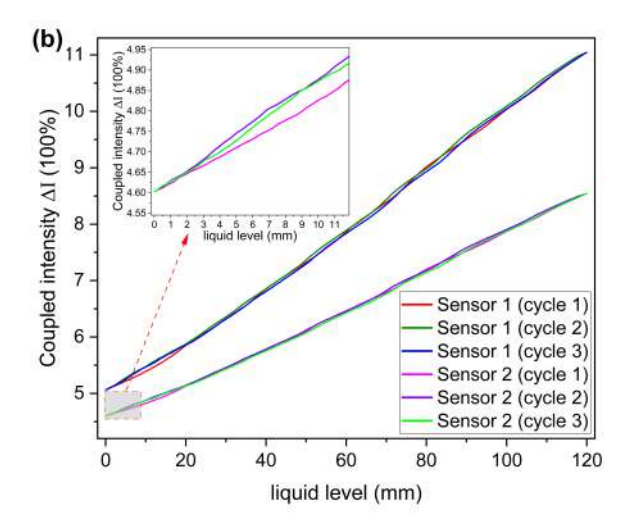


Fig. 7. Sensor-1 and sensor-2 repeatability tests. (a) while level ascending. (b) while level descending.

tal setup involved testing two sets of variable heights for both sensor-1 and sensor-2. Initially, the water tank was tilted to -35 degrees to the left, allowing sensor-2 to encounter the liquid level first, as illustrated in Fig. 2(c). Following this, the water tank was tilted to the right by 35 degrees, causing sensor-1 to more dipped with water as compare to sensor-2 because more water flow toward sensor-1, as schematic in Fig. 2(d). In the first experiment shown in Fig. 8(a), sensor-1 was positioned at half the elevation of sensor-2. When the tank was tilted to the right, sensor-2 began responding immediately as the liquid level rise from 0 mm, whereas sensor-1 only responded once the liquid level reached 45 mm. The response curves for both sensors demonstrated the effectiveness of the dual-point liquid level sensor in accurately capturing variations in liquid level under these conditions. Continuing with the second experiment shown in Fig. 8(b), the water tank was tilted to the left by 30 degrees, leading to sensor-1 responding first as the liquid level increased. Sensor-2 subsequently responded as the liquid continued to rise until it reached its position. The response curve for sensor-1 showed a decrease in power intensity once the liquid level reached a

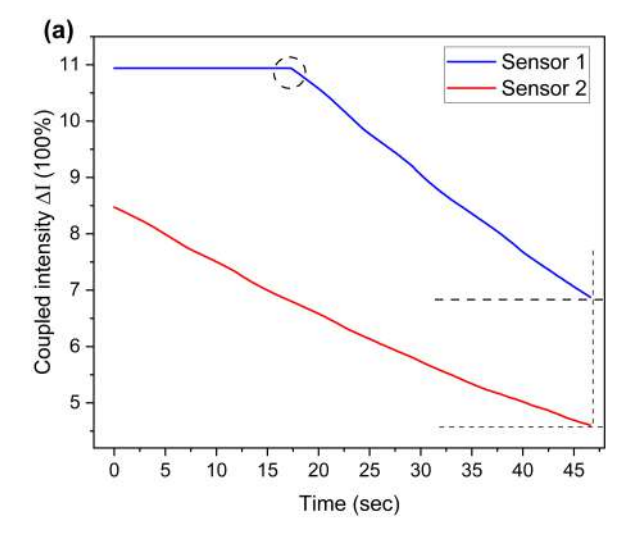
TABLE I
SENSITIVITY AND CORRELATION COEFFICIENTS FOR ASCENDING AND
DESCENDING CYCLES.

Cycle	Sensitivity (%/mm)	Y = ax + b	Correlation Coefficient (R <sup>2</sup> )
		Sensor 1 Ascending	
Cycle 1	0.050	-0.05033x + 10.79731	0.99691
Cycle 2	0.049	-0.04977x + 10.76731	0.99545
Cycle 3	0.049	-0.04965x + 10.72524	0.99471
	S	Sensor 1 Descending	
Cycle 1	0.051	0.05184x + 4.81799	0.99874
Cycle 2	0.051	0.05102x + 4.85958	0.99833
Cycle 3	0.051	0.05155x + 4.82917	0.99781
	;	Sensor 2 Ascending	
Cycle 1	0.033	-0.03314x + 8.37842	0.99572
Cycle 2	0.032	-0.03277x + 8.35499	0.99442
Cycle 3	0.032	-0.03269x + 8.33097	0.99494
	S	Sensor 2 Descending	
Cycle 1	0.033	0.03971x + 4.45039	0.99883
Cycle 2	0.034	0.03401x + 4.47419	0.99843
Cycle 3	0.033	0.03383x + 4.45435	0.99789

certain threshold. In contrast, the response curve for sensor-2 exhibited a continuous drop in power intensity from its initial level as the liquid level increased.

The continuous decrease in power intensity with respect to the rising liquid level for sensor-2 highlighted the full functionality of the sensor, considering its placement at the initial increase in liquid level height. Consequently, sensor-2 began to respond as the liquid level started to rise. These responses indicated that both sensors have independent reactions to changes in liquid level. Furthermore, the independent response of both sensors facilitated simultaneously measurement of liquid level at the different height. Additionally, the dual-sensor liquid level measurement could be applicable for simultaneously sensing different types of liquids. In this study, our proposed scheme is only tested for water. Although minor variations were observed in some measurement cycles, these were largely due to external handling and environmental conditions rather than fundamental limitations of the sensor design. For instance, the use of liquids with slightly different refractive indices resulted in only marginal power variations, which did not impact the overall sensitivity or accuracy. The dual-point configuration continued to function reliably under these changes, underscoring the system's robustness for typical use cases. Compared to more complex or rigid sensor designs, this approach offers a stable and practical solution for realworld liquid level monitoring.

The cost of sensor will be only depending on polymer optical fiber and casing. We are neglecting the cost of smartphone because in this era everyone has a smartphone. The dual-point liquid level sensor structure boasts several advantages, including flexibility, durability, cost-effectiveness, and active responsiveness to changes in liquid level. The sensors respond to liquid level variations through changes in optical power coupling due to alterations in the refractive



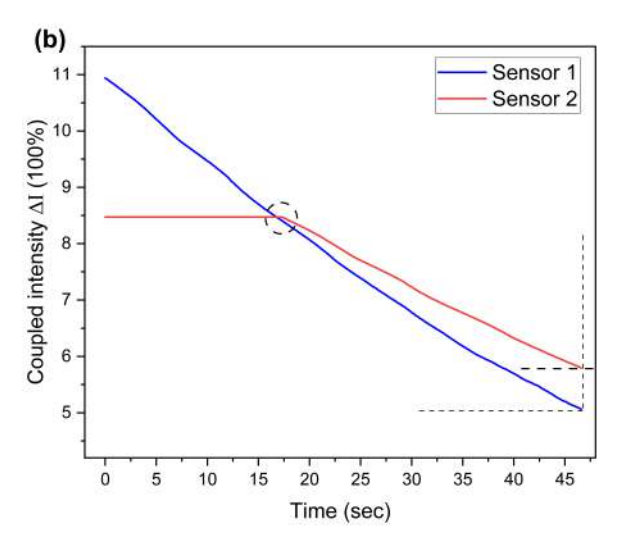


Fig. 8. Dual-sensor liquid level measurement response in the uneven ground situation. (a) response while the liquid tank is tilted in left by -35°. (b) response while the liquid tank is tilted in right side by 35°.

index. The primary advantage of the proposed dual-point liquid level sensor is its ability to measure and monitor liquid levels in various scenarios, including remote areas, even and uneven ground conditions, and different liquid types. These advantages make the proposed dual-point liquid level sensor valuable in applications where localized variations in liquid level may have significant implications for process control, safety, and efficiency. Moreover, the use of POF in the sensor design offers several benefits, such as being inexpensive, lightweight, and resistant to electromagnetic interference. The performance of the dual-point liquid level sensor system can be evaluated based on its accuracy, sensitivity, response time, and reliability. Overall, this work's dual-point liquid level sensor system represents a significant advancement in dual-point and portable liquid level sensing technology. Its innovative design, based on twisted POF, offers a versatile and reliable solution for measuring and monitoring liquid levels in real-time, with potential applications across a broad range of industries and environments.

#### IV. CONCLUSION

In this study, we developed a portable dual-sensor liquid level measurement using POF with a twisted structure for reliable and accurate liquid level monitoring in both closed and open systems. The sensor design integrates two probes, each capable of independently detecting liquid level changes, enabling high-resolution liquid level measurements. Both sensors exhibited linear responses to increasing and decreasing liquid levels, with a high degree of repeatability and accuracy. The dual-point sensor demonstrated excellent performance in various ground conditions, showing consistent measurements on both even and uneven surfaces. In even-ground setups, both sensors measured liquid levels from 0 to 120 mm, while in uneven conditions, sensor-1 detected variations after a 45 mm liquid rise, with sensor-2 measuring the entire range. Similarly, sensor-2 detected the liquid level ascending after 45 mm liquid rise, with sensor-2. This innovative sensor design offers a cost-effective, portable solution for real-time liquid level monitoring, with potential applications in industries such as environmental monitoring, chemical processing, and industrial safety.

#### REFERENCES

- [1] M. Wei, Z. Deng, J. Zheng *et al.*, "Magnetic float liquid level detection method for high-temperature superconducting flux-pinning maglev system," *IEEE Trans. Appl. Supercond.*, vol. 32, no. 4, pp. 1-5, 2022.
- [2] S. C. Bera, H. Mandal, S. Saha et al., "Study of a modified capacitancetype level transducer for any type of liquid," *IEEE Trans. Instrum. Meas.*, vol. 63, no. 3, pp. 641-649, 2014.
- [3] P. Esmaili, F. Cavedo, and M. Norgia, "Characterization of pressure sensor for liquid-level measurement in sloshing condition," *IEEE Trans. Instrum. Meas.*, vol. 69, no. 7, pp. 4379-4386, 2020.
- [4] J. Terzic, C. R. Nagarajah, and M. Alamgir, "Fluid level measurement in dynamic environments using a single ultrasonic sensor and Support Vector Machine (SVM)," Sens. Actuators A: Phys., vol. 161, no. 1, pp. 278-287, 2010.
- [5] L. F. Shi, W. Yin, Y. F. Lv et al., "An improved radar echo signal processing algorithm for industrial liquid level measurement," *IEEE Trans. Instrum. Meas.*, vol. 71, pp. 1-8, 2022.
- [6] J. R. Hanni, and S. K. Venkata, "A novel helical electrode type capacitance level sensor for liquid level measurement," Sens. Actuators A: Phys., vol. 315, 2020, Art. no. 112283, .
- [7] H. Canbolat, "A novel level measurement technique using three capacitive sensors for liquids," *IEEE Trans. Instrum. Meas.*, vol. 58, no. 10, pp. 3762-3768, 2009.
- [8] C. A. F. Marques, G.-D. Peng, and D. J. Webb, "Highly sensitive liquid level monitoring system utilizing polymer fiber Bragg gratings," *Opt. Exp.*, vol. 23, no. 5, pp. 6058-6072, 2015.
- [9] S. Hussain, A. Ghaffar, M. Mehdi et al., "Water waves detection by utilizing optical fiber surface microchannel sensor," Opt. Laser Technol., vol. 188, 2025 Art. no. 112918.
- [10] J. Zhao, R. Liu, M. Wang et al., "Integrated hybrid optical fiber Mach-Zehnder interferometers for simultaneous measurement of seawater temperature and salinity," Sens. Actuators A: Phys., vol. 380, 2024, Art. no. 116065.
- [11] X. Yang, B. Luo, D. Wu et al., "Simultaneous measurement of liquid level and refractive index based on a sandwich multimode optical fiber structure," Opt. Laser Technol., vol. 168, 2024, Art. no. 109856.
- [12] B. Xu, Y. Yang, Z. Jia *et al.*, "Hybrid Fabry-Perot interferometer for simultaneous liquid refractive index and temperature measurement," *Opt. Exp.*, vol. 25, no. 13, pp. 14483-14493, 2017.
- [13] C. A. R. Díaz, A. G. Leal-Junior, P. S. B. André et al., "Liquid level measurement based on FBG-embedded diaphragms with temperature compensation," *IEEE Sens. J.*, vol. 18, no. 1, pp. 193-200, 2018.
- [14] S. Rizzolo, J. Périsse, A. Boukenter et al., "Real time monitoring of water level and temperature in storage fuel pools through optical fibre sensors," Sci. Rep., vol. 7, no. 1, 2017, Art. no. 8766.

- [15] R. Fan, Q. Ma, L. Li et al., "Liquid level and refractive index double-parameter sensor based on tapered photonic crystal fiber," J. Lightw. Technol., vol. 38, no. 14, pp. 3717-3722, 2020.
- [16] M. S. U. K. Haider, C. Chen, A. Ghaffar et al., "Simultaneous measurement of liquid level and R.I. sensor using POF based on twisted structure," Sci. Rep., vol. 15, no. 1, 2025, Art. no. 1163.
- [17] J. Wang, L. Wang, X. Su et al., "Temperature, stress, refractive index and humidity multi parameter highly integrated optical fiber sensor," Opt. Laser Technol., vol. 152, 2022, Art. no. 108086.
- [18] L. Kong, X. Du, C. Ren et al., "Lab-in-fibers: Single optical fiber with three channels for simultaneous detection of pH value, refractive index and temperature," Sens. Actuators B: Chem., vol. 385, 2023, Art. no. 133727.
- [19] M. Elsherif, A. E. Salih, M. G. Muñoz et al., "Optical fiber sensors: Working principle, applications, and limitations," Adv. Photon. Res., vol. 3, no. 11, 2022, Art. no. 2100371.
- [20] J. Du, Z. Gu, Q. Ling et al., "Design of an anti-temperature interference liquid level sensor based on tilt long-period fiber grating," Opt. Laser Technol., vol. 177, 2024, Art. no. 111229.
- [21] C. W. Lai, Y. L. Lo, J. P. Yur et al., "Application of fiber bragg grating level sensor and Fabry-Pérot pressure sensor to simultaneous measurement of liquid level and specific gravity," *IEEE Sens. J.*, vol. 12, no. 4, pp. 827-831, 2012.
- [22] A. L. Ricchiuti, D. Barrera, A. Urrutia et al., "Continuous liquid-level sensor based on a long-period grating and microwave photonics filtering techniques," *IEEE Sens. J.*, vol. 16, no. 6, pp. 1652-1658, 2016.
- [23] B. Haiyang, and Z. Jie, "Liquid-level sensor based on flat-shaped plastic optical fiber assisted by a long-period grating," Proc. SPIE, 2024, vol. 13243, pp. 142-148.
- [24] M. Sun, Y. Jin, and X. Dong, "All-fiber Mach–Zehnder interferometer for liquid level measurement," *IEEE Sens. J.*, vol. 15, no. 7, pp. 3984-3988, 2015.
- [25] W. Zhang, X. Wu, G. Zhang et al., "An inline Mach-Zehnder interferometer for simultaneously measuring liquid level and temperature," Opt. Fiber Technol., vol. 63, 2021, Art. no. 102501.
- [26] P. Mohindru, "Development of liquid level measurement technology: A review," Flow Meas. Instrum., vol. 89, 2023, Art. no. 102295.
- [27] R. He, C. Teng, S. Kumar et al., "Polymer optical fiber liquid level sensor: A review," IEEE Sens. J., vol. 22, no. 2, pp. 1081-1091, 2022.
- [28] M. S. U. K. Haider, C. Chen, A. Ghaffar et al., "Smartphone-based optical fiber sensor for refractive index sensing using POF," Sens. Actuators A: Phys., vol. 385, 2025, Art. no. 116321.
- [29] J. Park, Y. J. Park, and J. D. Shin, "Plastic optical fiber sensor based on in-fiber microholes for level measurement," *Jpn. J. Appl. Phys.*, vol. 54, no. 2, 2015, Art. no. 028002.
- [30] Y. Zhang, Y. Hou, Y. Zhang et al., "A multipoint liquid level sensor based on two twisted polymer optical fibers in a race-track helical structure," J. Sens., vol. 2018, no. 1, 2018, Art. no. 4914382.
- [31] K. Liao, Y. Li, M. Lei et al., "A liquid level sensor based on spiral macro-bending plastic optical fiber," Opt. Fiber Technol., vol. 70, 2022, Art. no. 102874.
- [32] M. S. U. K. Haider, C. Chen, A. Ghaffar et al., "Portable optical fiber sensor for continuous liquid level sensing using commercially available POF," *IEEE Sens. J.*, vol. 25, no. 3, pp. 4582-4589, 2025.
- [33] X. Liang, Y. Long, K. Xiang et al., "Smartphone-integrated POF speckle sensor for heart rate variability monitoring," *IEEE Sens. Lett.*, vol. 8, no. 10, pp. 1-4, 2024.
- [34] Q. Q. Sun, C. Zhu, Z. Z. Hu et al., "Design and signal processing of plastic optical fiber respiratory sensors based on smartphones," Opt. Fiber Technol., vol. 84, 2024, Art. no. 103752.
- [35] Y. Ye, C. Zhao, Z. Wang et al., "Portable multihole plastic optical fiber sensor for liquid-level and refractive index monitoring," *IEEE Sens. J.*, vol. 23, no. 3, pp. 2161-2168, 2023.
- [36] C. Zhao, Y. Ye, Z. Wang et al., "Notch POF integrated with smartphone for liquid level and refractive index monitoring," Opt. Laser Technol., vol. 167, 2023, Art. no. 109751.
- [37] D. Marcuse, "Derivation of coupled power equations," Bell Syst. Tech. J., vol. 51, no. 1, pp. 229-237, 1972.
- [38] D. Marcuse, "Coupled power equations for backward waves," *IEEE Trans. Microw. Theory Tech.*, vol. 20, no. 8, pp. 541-546, 1972.
- [39] "Specification sheet of high-performance plastic optical fiber, Mitsubishi Rayon Co., LTD 6-41 konan 1-chome, minato-ku, Tokyo, Japan."
- [40] F. Kimme, P. Brick, S. Chatterjee et al., "Optimized flash light-emitting diode spectra for mobile phone cameras," *Appl. Opt.*, vol. 52, no. 36, pp. 8779-8788, Dec. 2013.

[41] A. Friedrichs, J. A. Busch, H. J. Van der Woerd et al., "SmartFluo: A Method and Affordable Adapter to Measure Chlorophyll a Fluorescence with Smartphones," *Sensors*, vol. 17, 2017, Art. no. 678.